Atomic and electronic structures, elastic properties, and optical conductivity of bulk Te and Te nanowires: A first-principles study

Prasenjit Ghosh, Mousumi Upadhyay Kahaly, and Umesh V. Waghmare
Theoretical Sciences Unit, Jawaharlal Nehru Centre for Advanced Scientific Research, Jakkur P.O., Bangalore 560 064, India
(Received 12 September 2006; revised manuscript received 1 March 2007; published 29 June 2007)

We present a comparative study of atomic and electronic structures, Young's modulus, and optical conductivity of trigonal bulk tellurium and its nanowires of different diameters using first-principles density-functional theory calculations based on pseudopotentials and a generalized gradient approximation to exchange-correlation energy. Bulk trigonal Te consists of parallel helices of Te stacked on a triangular lattice in a plane perpendicular to the helical axis. In Te nanowires, interhelical distances change by about 1% of their bulk value due to rearrangement of atoms at the surfaces. Due to a decreased overlap between electronic states of neighboring helices, band gap of nanowires increases with reducing diameter, whereas their Young's modulus correspondingly decreases. Optical conductivity of nanowires depends on their diameter and exhibits a marked anisotropy due to quantum confinement of electronic states in the plane perpendicular to their axis.

DOI: 10.1103/PhysRevB.75.245437 PACS number(s): 71.15.−m, 71.20.−b, 71.23.An

I. INTRODUCTION

One-dimensional nanostructures such as nanowires, nanorods, or nanotubes have been a subject of intensive research for the past few years due to their potential use as interconnects and active components in fabricating nanoscale electronic or optoelectronic devices.[1] They represent interesting systems for investigating the dependence of optical, electrical, electrochemical, and mechanical properties on size.[2] There has been a surge in research activities related to synthesis, characterization, and theoretical studies of nanowires of various inorganic materials such as oxides, sulfides, and nitrides as well as elemental metals.

One of the elemental materials of interest is tellurium (Te) which has several interesting physical and chemical properties such as photoconductivity, thermoelectric effect, nonlinear optical responses, and catalytic activity,[3] which make it useful in applications such as electronic and optoelectronic devices and xerography.[4] Unlike other elements of group VI (O, S, Se), bulk Te exhibits only one crystalline form, namely, trigonal. The crystal structure of *t*-Te consists of parallel helical chains stacked on a triangular lattice, with their axes parallel to the crystalline *c* axis. The space groups of the crystal are D_3^4 and D_3^6 depending on the sense of rotation of the helical chain. Structure and properties of Te show anisotropy (though less than the isostructural trigonal selenium) which arises from the disparity between a strong covalent bonding between neighboring atoms belonging to a single helix (intrachain) and a relatively weaker bonding interaction between atoms on the neighboring chains (interchain).

Recently, research groups have synthesized nanowires and nanotubes of *t*-Te.[5–7] The availability of Te nanowires has opened up possibilities of new types of applications and has made it important to know how the properties of Te nanowires depend on their diameter and affect their performance in the present devices. Fundamentally, it is interesting to understand the stability of Te nanowires as bundles of helices and how the quantum size effects manifest in the size dependence of their properties.

In this work, we use first-principles calculations to determine the atomic and electronic structures and various properties of bulk Te, its nanowires, and a single helix. In Sec. II, we describe details of the first-principles calculations and results for the bulk to benchmark our calculations through comparison with earlier first-principles calculations and experiments. A comparative study of atomic structures, binding energy, and Young's modulus is presented in Sec. III. We present the study of size dependence of electronic structures in Sec. IV. We report and discuss results for optical conductivity in Sec. V and summarize in Sec. VI.

II. METHODS

We used the ABINIT (Refs. 8 and 9) package, an implementation of the density-functional theory,[10] based on first-principles optimized pseudopotential and a generalized gradient approximation of the exchange-correlation energy given by the Perdew-Burke-Ernzerhof (PBE) functional.[11–14] Our calculations are based on the solution of the Kohn-Sham equations[15] by fixed potential-based iterative conjugate-gradient minimizations[16] of one-electron energies and a mixing of potentials toward self-consistency. Optimized pseudopotentials[17] were constructed using the OPIUM (Ref. 18) and treating six electrons in the outermost *s* and *p* states as valence with cutoff radius of 2.1 Å and optimizing wave vector of 5.5 a.u. An energy cutoff of 30 Ry was used on a plane-wave basis converging total energies within 1 mRy per atom.

We simulated bulk Te (3 atoms/cell), a double-shelled Te nanowire (Te-w2) with 57 atoms per cell and a diameter of about 22 Å, a single-shelled Te wire (Te-w1) with 21 atoms per cell and a diameter of about 14 Å, and a single helix (Te-h) with 3 atoms per cell and a diameter of about 3.2 Å. The nanowires and helix are periodic in the *c* direction but are confined in the *ab* plane. We used hexagonal supercells with the in-plane lattice parameter *a* up to 40 Å, with a vacuum of about 10 Å separating the periodic images of the nanowires. This ensures negligible interaction between the periodic images.

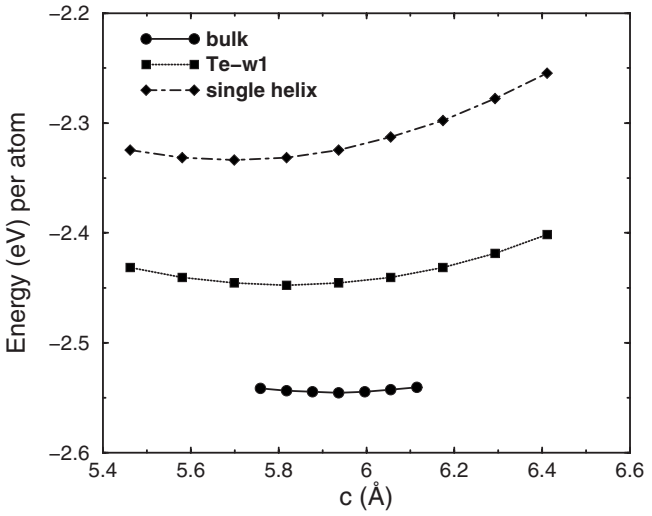

FIG. 1. Cohesive energy per atom (with a negative sign) vs lattice constant c for bulk Te, Te-w1, and a helix.

Integrations over the Brillouin zone were evaluated with a $5\times5\times5$ Monkhorst-Pack mesh[19] [19 k points in the irreducible Brillouin zone (IBZ)] for bulk Te and $1\times1\times5$ grid (3 k points in IBZ) for the wires of different diameters and the helix, with total energies converging within 2 meV/atom. As Te is known to be semimetallic, we use smearing of occupation numbers of states with a Gaussian function, corresponding to the zeroth-order Hermite polynomial of Methfessel and Paxton,[20] with a smearing temperature of 473 K for bulk Te and Te-h and 1136 K for Te-w1 and Te-w2. Structural optimization was carried out using the Hellmann-Feynman forces and the Broyden-Fletcher-Goldfarb-Shanno-based method[21] for the minimization of energy.

Structure of bulk Te is characterized by three parameters: a, c/a ratio, and a reduced coordinate u giving the position of atoms projected onto the ab plane from the axis of the helix; c is also the pitch of the helical chains. Structural optimization is carried out by keeping c fixed and relaxing a and u to minimize the total energy. Cohesive energy of a given Te structure is obtained by subtracting the total energy of free Te atoms from the total energy of the structure. In order to test the importance of zero-point motion, we calculate the contribution of zero-point motion to the total energy of bulk Te. We find that the zero-point motion changes the total energy of Te bulk by about 5 meV. These changes are so small that they do not affect the equilibrium geometry. Henceforth, in our calculations, we will neglect the contributions to the total energy from zero-point motion. From the cohesive energy as a function of c (Fig. 1), the minimum energy structure and Young's modulus are readily obtained (Table I). Our calculations yield a bulk structure that is slightly overbound than the earlier calculation of Kresse *et al.*,[28] reflected in higher cohesive energy and bulk modulus, and smaller volume. Our estimates of the unit-cell volume and the c/a ratio are in closer agreement with the experiment. The internal structural parameter u is overestimated by 4.5% with respect to the experimental value, translating into similar errors in the ratio of interchain to intrachain distances (d_2/d_1) and the intrachain Te-Te-Te bond angle (θ).

III. STRUCTURE, COHESIVE ENERGY, AND YOUNG'S MODULUS OF Te NANOWIRES

The cohesive energies (Fig. 1) clearly bear that bulk Te is most stable whereas Te-h is least stable. Coordination number of atoms in the bulk Te is 6, whereas it reduces to 2 in the case of a helix. Due to the lower coordination of atoms at the surface of nanowires, intrachain bond lengths are shorter (see Table II) and hence their c parameter reduces with reducing diameter. As the presence of a surface in a nanowire costs energy and the fraction of atoms at the surface increases with reducing diameter, the cohesive energy per atom correspondingly reduces from 2.54 eV/atom of the bulk to 2.33 eV/atom of the helix.

The radius of a nanowire is an important parameter because estimation of many properties of the nanowires such as surface energy, Young's modulus, etc., is sensitive to this radius. There are many ways of defining the radii of nanowires,[22–24] which depend on their atomic radii, bond lengths, or charge distribution. We define here the radius of a wire R as the radius of a cylinder in which 99% of the total electronic charge in the system is enclosed, i.e., $\int_0^R\int_0^c\rho(r)2\pi r dz dr=0.99eN_e$, where $\rho(r)$ and N_e are the charge density and the total number of electrons in the system, respectively. Consistent with the reduction in the c parameter, radius per helix of nanowires is found to increase with reducing diameter (given in Table II).[25]

We calculate the surface energy per unit area (γ_s) of nanowires which is defined as

$$\gamma_s = \frac{E_{NW} - n_{NW}E_{bulk}}{A} \tag{1}$$

where E_{NW} and n_{NW} represent the total energy and the number of atoms of a nanowire respectively. E_{bulk} denotes the

TABLE I. Comparison of minimum-energy structure (unit cell-volume Ω, c/a, internal structure parameter u, bond angle (θ), and ratio d_2/d_1 of interchain and intrachain distances), bulk modulus (B), and cohesive energy (E) of Te with experiments and other calculations.

	Ω (Å^3)	c/a	u	d_2/d_1	θ (deg)	B (Kbar)	E (eV/atom)
PBE (This work)	33.95	1.33	0.276	1.18	101.3	330	2.54
PB-Kresse (Ref. 28)	36.11	1.31	0.269	1.21	101.0	180	2.35
Experimental (Refs. 29 and 30)	33.74	1.33	0.264	1.23	103.0	230	2.19

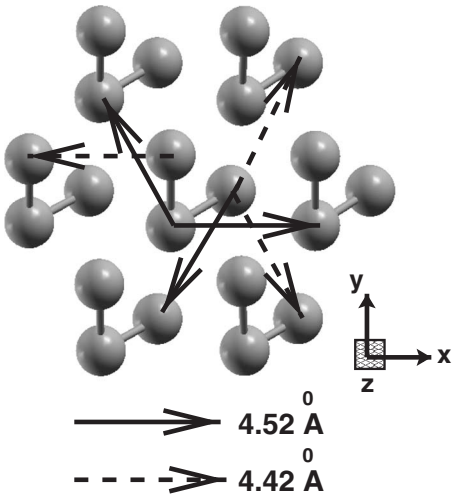

FIG. 2. Variation of interhelical distances d of Te-w1 due to surface effect.

energy of a Te atom in bulk and A $(=2\pi Rc)$ is the surface area of the nanowire. Surface energies of Te-w2, Te-w1, and Te-h are 0.14, 0.12, and 0.09 J/m^2, respectively.

Unlike bulk Te, which is a periodic lattice of helices, different helices of Te-w1 and Te-w2 are not identical. For example, while the point symmetry of Te-w1 nanowire is the same as that of the bulk (space group $P3_221$), the helices at its surface form two groups of three identical helices each, maintaining the threefold rotational symmetry. Structural relaxation through displacements of Te atoms in the ab plane results in variation of bond lengths and bond angles, listed in Table II. The distance between a helix from the first group (marked by solid arrows in Fig. 2) and the central helix of Te-w1 d increases by 1.6%, while that from the second group (marked by dashed arrows in Fig. 2) decreases by 0.7%. While the structure of the helix at the center of Te-w1 is unchanged and its bond lengths remain the same as those in the bulk Te (2.91 Å), Te-Te bond lengths of Te atoms in helices at the periphery change due to structural relaxation. For the first group of helices (marked by the solid arrows), relaxation results in two short (2.74 Å) and one long (2.86 Å) bonds, whereas it leads to two long (2.86 Å) and one short (2.79 Å) bonds in the second set of helices. In a given ab plane, the long bonds of the former line up with the short bonds of the latter. For both the group of helices, atoms come close to each other compared to those of the bulk, resulting in the contraction of Te-w1 along the c axis. Similar features are observed in the helices of Te-w2.

In order to estimate the strength of nanowires and compare them with that of the bulk, we determine their Young's modulus Y:

$$Y = \frac{1}{V_0} \left. \frac{\partial^2 E}{\partial \epsilon_{zz}^2} \right|_{\epsilon_{zz}=0}, \tag{2}$$

where E is the relaxed total energy and ϵ_{zz} is the strain applied on the system $\left(=\frac{\delta c}{c}\right)$ at an equilibrium volume V_0. The wires are treated as cylinders with radii R as defined earlier in this section and their volume per unit cell is given by $V_0 = \pi R^2 c$. Young's modulus of bulk Te is 45.8 GPa, in close agreement with an experimental estimate of 43 GPa.[26] Our calculations predict that Y reduces, with reducing diameter, to 35.1 and 28.5 GPa for the Te-w1 and the helix, respectively. Earlier in this section, we showed that the intrachain bond lengths in the nanowires are shorter than those in bulk. This implies stronger intrachain bonds in nanowires. If the helices in nanowires or bulk were noninteracting, Young's modulus of the nanowires would have been higher than that of bulk.[27] Smaller Young's modulus of nanowires is clearly an effect of changes in the bonding between atoms in different helices. For the bulk Te, each helix is surrounded by six nearest-neighbor helices, whereas a helix at the surface of Te-w1 has only three neighboring helices and its separation from the neighboring helices is different than that in bulk. This results in fewer and weaker bonds between atoms in neighboring helices particularly at the surface of nanowires and hence their lower Young's moduli.

IV. ELECTRONIC STRUCTURE

Our calculated electronic structure of bulk Te (Fig. 3) compares quite well with earlier calculations.[31,37] Valence bands occur in two groups: (i) VB1, with a bandwidth of about 5.5 eV, and (ii) VB2, higher in energy than VB1, with a bandwidth of 6.0 eV. The conduction band forms a continuum of states. The band VB2 and the conduction band are separated by a tiny direct gap of 0.15 eV at the H point, the experimental value of band gap being 0.33 eV.[32] This is consistent with typical underestimation of gaps in the density-functional theory (DFT) calculations.

Band structure and density of states (DOS) of Te-h (Fig. 4) show five distinct bands: (i) three valence bands [VB1,

TABLE II. Comparison of structural parameters, cohesive energy (E), and Young's modulus (Y) of bulk Te, Te-w2, Te-w1, and Te-h. R, R_{helix}, d, and θ are the radii of nanowires, radius of each helix constituting the bulk and the nanowires $[R_{helix}=(n)^{1/2}R$, n is the number of helices for each nanowire], interhelical distances, and Te–Te–Te intrahelix bond angle, respectively.

System	R (Å)	R_{helix} (Å)	d (Å)	c (Å)	θ (deg)	Bond length (Å)	E (eV/atom)	Y (GPa)
Bulk		2.3	4.45	5.93	101.3	2.91	2.54	45.8
Te-w2	10.98	2.52	4.45,4.52	5.86	98.9–105.1	2.74–2.9	2.48	
Te-w1	6.88	2.6	4.42,4.52	5.82	98.3–104.1	2.74,2.79,2.85,2.86,2.91	2.44	35.1
Te-h	3.2	3.2		5.69	102.7	2.74	2.33	28.5

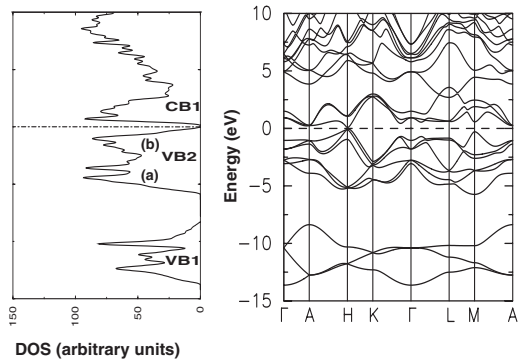

FIG. 3. Electronic structure of bulk Te along high-symmetry directions in the BZ of a hexagonal lattice (right panel). Density of states (DOS) of electrons is given in the left panel.

VB2(a), and VB2(b)] and (ii) two conduction bands [CB1(a) and CB2(b)]. The bands are flat, resulting in sharp Van Hove singularities in the DOS. For the nanowires (Te-w1 and Te-w2), if the neighboring helices are not interacting, the band structure would have been identical to that of Te-h. The interaction between neighboring helices of Te-w1 and Te-w2 causes an increase in overlap of the wave functions, as a consequence of which the bandwidth increases. This is evident from Figs. 4–6. For example, in Te-h, VB2 consists of two bands, VB2(a) and VB2(b), while for the wires they merge into one band, namely, VB2. The bandwidths of VB1 and VB2 bands of Te-w1 and Te-w2 are close to those of bulk Te, while those of Te-h are smaller (Table III). An increase in the bandwidth of the bands results in a decrease of the band gaps with increasing thickness of the nanowires, which is consistent with the experimental findings.[5] Band gaps for all the three cases, namely, Te-h, Te-w1, and Te-w2, are indirect ones.

Conduction bands of the nanowires, CB1, also show significant variations from that of the bulk. In bulk Te, CB1 forms a continuum with an infinite bandwidth. For the wires and Te-h, CB1 splits into two bands, CB1(a) and CB2(b), the bandwidth of CB2(b) for Te-h being infinite. For Te-w2, bands beyond 2.0 eV have not been obtained because of the intensive computational efforts involved.

The isosurfaces of charge density for Te-h arising from the states (−15 to 2.5 eV) at the Γ point of the BZ are shown

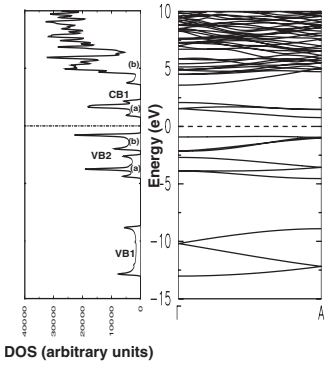

FIG. 4. Density of states and electronic structure of Te-h. "a" and "b" denote the different subbands of VB2 and CB1.

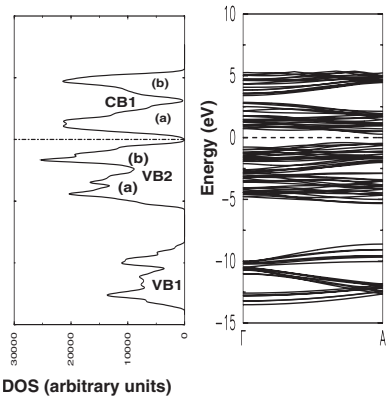

FIG. 5. Density of states and electronic structure of Te-w1. "a" and "b" denote the different subbands of VB2 and CB1. VB2(a) and VB2(b) merge into one band.

in Fig. 7. The VB1 band [Fig. 7(a)] describes electrons of predominantly *s* orbital character with slight mixing with the *p* orbital. Figures 7(b) and 7(c) show the *p*-bonding and the *p*-lone-pair orbital character of the electrons. The electrons from *p*-antibonding orbital (with slight mixing of *s* orbital) are shown in Fig. 7(d). For Te-w1, Te-w2, and bulk Te, the isosurfaces show similar features because the interactions between the atoms in the neighboring helices are very weak compared to intrahelical interactions.

V. OPTICAL CONDUCTIVITY

Optical conductivity of nanowires strongly depends on their diameter and the direction of polarization of the incident light. We used the Kubo-Greenwood[34,35] formula to compute the optical conductivity tensor:

$$\sigma_{\alpha\beta}(\omega) = \frac{2\pi}{3\omega}\int_{BZ} dk \Sigma_{i,j}(f_i^k - f_j^k)\left|\left\langle \psi_i^k \left| \frac{\partial}{\partial x_\alpha} \right| \psi_j^k \right\rangle \times \left\langle \psi_i^k \left| \frac{\partial}{\partial x_\beta} \right| \psi_j^k \right\rangle\right| \delta(\varepsilon_j^k - \varepsilon_i^k - \omega), \quad (3)$$

where f_i^k is the Fermi-Dirac occupation, ω is the energy of

TABLE III. Summary of band-structure results. "a" and "b" denote the different VB2 and CB1 of Te-h and Te-w1, as shown in Figs. 4 and 5, respectively.

		Bandwidth (eV)		
System	Band gap (eV)	VB1	VB2	CB1
Te bulk	0.15	5.44	5.83	∞
Te-w2	0.45	5.42	5.81	1.65
Te-w1	0.75	5.40	5.62	3.1 for (a) 2.6 for (b)
Te-h	1.64	4.43	2.21 for (a) 1.53 for (b)	1.63 for (a) ∞ for (b)

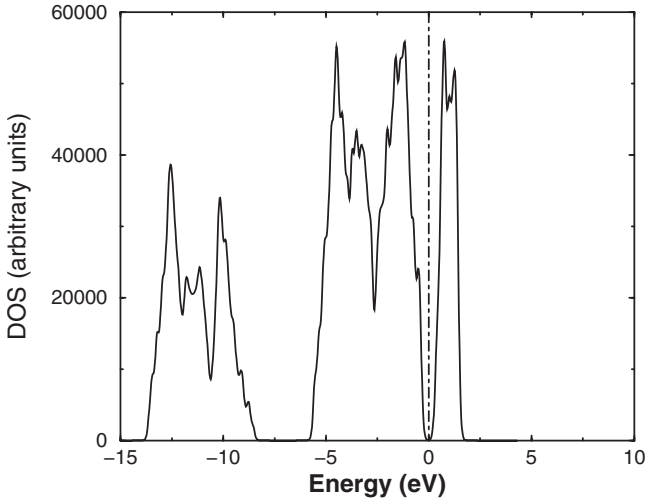

FIG. 6. Density of states of Te-w2.

the incident photon, ε_i^k and $|\psi_i^k\rangle$ are the energy eigenvalue and the energy eigenfunction of the ith band at the Bloch wave vector k, x_α is the α component of position vector $\mathbf{r}$, and $\langle \psi_i^k | \frac{\partial}{\partial x_\alpha} | \psi_j^k \rangle$ is the interband transition matrix element. Eigenvalues of σ yield the optical conductivity along the three principal axes. The transition matrix elements are obtained using d/dk linear-response module of the ABINIT code.[8] Whenever the energy of an incident photon matches a Van Hove singularity in the DOS, subject to the selection rules given by the interband transition matrix element and the Pauli's exclusion principle, there is a resonant enhancement in the optical conductivity giving rise to its peaks. In our calculations of σ and the imaginary part of the dielectric constant [see Eq. (4) and Fig. 9 later], we employ a smoothening technique that replaces the delta function in Eq. (3) with a Gaussian of width 0.01 eV.

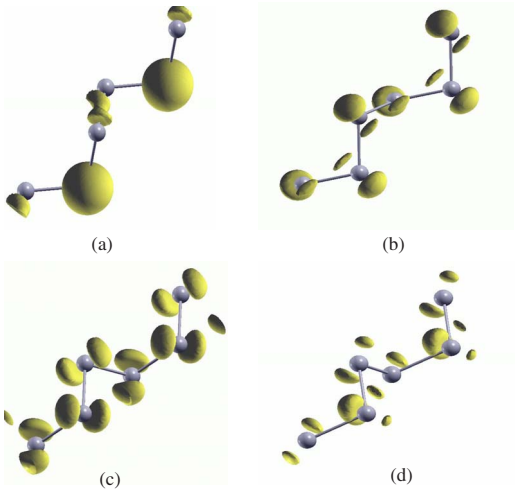

FIG. 7. (Color online) Isosurfaces of charge density for Te-h. The isovalue corresponding to the isosurfaces is 50% of the maximum isovalue. (a), (b), (c), and (d) are for VB1, VB2(a), VB2(b), and CB1(a), respectively. The helices are aligned such that the z axis is parallel to the axis of the helix. These pictures have been generated using a software called XCRYSDEN (Ref. 33).

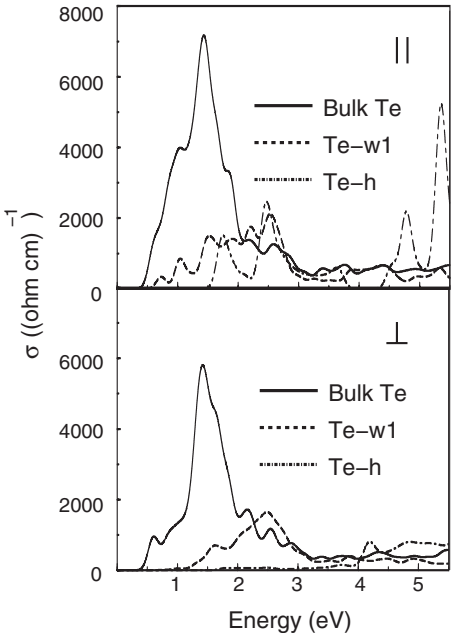

FIG. 8. Optical conductivity plot for bulk Te, Te-w1, and a single helix at 300 K for two directions of polarization of E: (a) $E \| c$ and (b) $E \perp$ to c.

Optical properties of bulk Te depend on the direction of polarization of incident light with respect to the c axis. The three principal components of the conductivity tensor are (i) σ_{cc}, along the c axis, when the polarization direction of incident light and the current are parallel ($\|$) to the c axis, and (ii) $\sigma_{aa}=\sigma_{bb}$ (from crystal symmetry $a=b$), i.e., when the polarization of incident light and current are perpendicular ($\perp$) to c. For both directions of polarization, there is a distinct peak at around 1.43 eV (see Fig. 8). In addition to this peak, σ of bulk Te exhibits a hump at about 0.61 eV and a shoulder at about 1.03 eV when the polarization of incident light is $\|$ to c, and a peak at about 0.61 eV when the polarization of incident light is $\perp$ to c.

To compare our results with experimental data and other theoretical calculations, we compute the imaginary part of the dielectric constant $[\epsilon_{im}(\omega)]$:

$$\epsilon_{im}(\omega) = \frac{4\pi}{\omega}\sigma^{real}(\omega). \tag{4}$$

Our results (see Fig. 9) are in good agreement with the experiments performed by Tutihasi *et al.*[36] except for the facts that (i) the theoretical peak is redshifted by about 0.5 eV and (ii) the value of ϵ_{im} corresponding to the peak is nearly twice that of the experimental value. To understand the origin of differences in the estimates of ϵ_{im} obtained from experiment and our calculations, we separate out the effects of the matrix elements and the density of states on ϵ_{im}. We determine the joint density of states (JDOS), given by the convolution of electronic DOS. From the comparison of JDOS with the work of Starkloff and Joannopoulos,[37] we find the interband transitions that give rise to various peaks. Overall features of the JDOS obtained from our calculations agree fairly well with those of Starkloff and Joannopoulos. The redshift in the

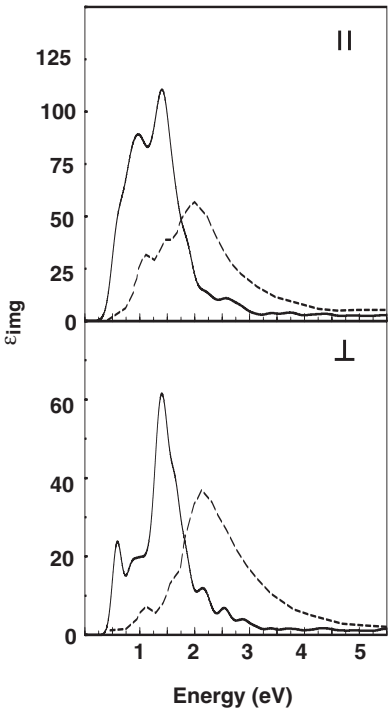

FIG. 9. Imaginary part of dielectric constant ϵ for bulk Te at 300 K: the upper and lower panels show ϵ when polarization directions of incident light are $\parallel$ and $\perp$ to c, respectively. The solid line shows the theoretically calculated ϵ, while the dashed ones are the experimentally measured values (Ref. 36).

position of peaks and the factor of about 2 in the value ϵ_{im} corresponding to these peaks primarily arise from the underestimation of the band gap, typical of DFT calculations. While our calculations predict a band gap of 0.15 eV, the experimentally measured value of band gap is 0.33 eV. We note that our finding of the peak in ϵ_{im} at 1.43 eV is consistent with previous experimental measurements[36] and calculations,[37] though it was not observed in the absorption spectra of bulk Te by Goutam and Rao.[5]

For nanowires, the splitting of bands results in sharper peaks than that of the bulk. Optical conductivities of Te-w1 and Te-h (Fig. 8) for polarization along the c axis exhibit many peaks. Positions of the peaks in σ for these two systems and the corresponding interband transitions are listed in Table IV. For both the directions of polarization of incident light, there is a significant decrease in the magnitude of σ in comparison to that of bulk, which can be largely explained by the changes in the band gap. In contrast to bulk Te and Te-w1, Te-h shows two distinct peaks at 4.8 and 5.4 eV, when the direction of polarization of incident light and the current are $\parallel$ to c (top panel of Fig. 8). These peaks correspond to the electronic transitions from VB2(a) to CB1(a) and their origin can be explained from the band structure of Te-h (right panel of Fig. 4). VB2(a) and CB1(a) being almost parallel cause an increase in the JDOS of Te-h, which results in the peaks in σ at the above-mentioned values of ω.

In contrast to bulk Te, optical conductivity spectra of the nanowires exhibit very strong dependence on the direction of polarization of the incident light. For polarization of light $\parallel$ to c, there are no peaks for Te-h below 1.49 eV (top panel of Fig. 8). Peaks seen in bulk and Te-w1 below 1.49 eV arise from the interchain hopping of electrons. Since Te-h has a single helix, there is no contribution in optical conductivity from interchain hopping of electrons, resulting in the absence of those peaks. The spectra for Te-h for σ_{aa} (lower panel of Fig. 8) show negligible optical conductivity below 4.0 eV, followed by a small peak at 4.19 eV, whereas Te-w1 and bulk show noticeable conductivity below 4 eV. This shows that the interchain interactions play a prominent role in the size dependence of σ_{aa} of nanowires.

TABLE IV. Transitions corresponding to different peaks in optical conductivity plot for $E \| c$.

System	Position of peak (eV)	Transitions
Bulk Te	0.61	VB2(b) → CB1
	1.03	
	1.43	
Te-w1	0.71	VB2(b) → CB1(a)
	1.03	
	1.53	
	1.90	
	2.20	
	2.52	
Single helix	1.75	VB2(b) → CB1(a)
	2.48	
	3.63	
	4.79	VB2(a) → CB1(a)
	5.36	

VI. SUMMARY

We have studied effects of the thickness of the nanowires of Te on their geometry, surface energy, Young's modulus, electronic structure, and optical conductivity using the *ab initio* density-functional theory calculations.

Reduction in the coordination number of the atoms at the surfaces of nanowires results in (a) rearrangement of atoms at the surface, (b) stronger intrahelical Te–Te bonds and reduction in the lattice parameter c with decreasing size, (c) changes in the interhelical distances d by approximately 1%, and (d) subsequently the reduction in Young's modulus. These structural changes correlate with decreasing overlap of electronic wave functions of different helices, and the electronic structure of nanowires exhibits a blueshift in the band gap with decreasing diameter of the wires. In contrast to the bulk Te, optical conductivity of its nanowires is strongly dependent on the direction of polarization of the incident light. Due to lack of hopping between helices, for light polarized perpendicular to its axis, optical conductivity of Te-h is significantly lower in comparison with those of other nanowires or bulk Te.

ACKNOWLEDGMENTS

We thank C. N. R. Rao, Joydeep Bhattacharjee, and Ujjal K. Goutam for useful discussions. P.G. acknowledges CSIR, India for a research scholarship. Most of the calculations were carried out on the central computing facility supported by JNCASR, Department of Science and Technology, Government of India.

[1] H. M. Huang, S. Mao, H. Feick, H. Yan, Y. Wu, H. Kind, E. Weber, R. Russo, and P. Yang, Science **292**, 1897 (2001); S.-W. Chung, J.-Y. Yu, and J. R. Heath, Appl. Phys. Lett. **76**, 2068 (2000).

[2] J. Hu, T. W. Odom, and C. Lieber, Acc. Chem. Res. **32**, 435 (1999); S. M. Prokes and K. L. Wang, MRS Bull. **24**, 13 (1999); Z. L. Wang, Adv. Mater. (Weinheim, Ger.) **12**, 1295 (2000).

[3] E. Gerlach and P. Grosse, *The Physics of Selenium and Tellurium* (Springer-Verlag, Berlin, 1979); E. D. Cooper, *Tellurium* (Van Nostrand Reinhold, New York, 1974).

[4] A. A. Kudryavstev, *The Chemistry and Technology of Selenium and Tellurium* (Collet's Ltd., London, 1974); P. Tangney and S. Fahy, Phys. Rev. B **65**, 054302 (2002).

[5] Ujjal K. Goutam and C. N. R. Rao, J. Mater. Chem. **14**, 2530 (2004).

[6] Z. Liu, S. Li, Y. Yang, Z. Hu, S. Peng, J. Liang, and Y. Qian, New J. Chem. **27**, 1748 (2003).

[7] Shaswati Sen *et al.* (private communication).

[8] X. Gonze, J.-M. Beuken, R. Caracas, F. Detraux, M. Fuchs, G.-M. Rignanese, L. Sindic, M. Verstraete, G. Zerah, F. Jollet, M. Torrent, A. Roy, M. Mikami, Ph. Ghosez, J.-Y. Raty, and D. C. Allan., Comput. Mater. Sci. **25**, 478 (2002); http://www.abinit.org.

[9] S. Goedecker, SIAM J. Sci. Comput. (USA) **18**, 1605 (1997).

[10] P. Hohenberg and W. Kohn, Phys. Rev. **136**, B864 (1964).

[11] J. P. Perdew, K. Burke, and M. Ernzerhof, Phys. Rev. Lett. **77**, 3865 (1996).

[12] J. P. Perdew, K. Burke, and M. Ernzerhof, Phys. Rev. Lett. **78**, 1396 (1997).

[13] Y. Zhang and W. Yang, Phys. Rev. Lett. **80**, 890 (1998).

[14] J. P. Perdew, K. Burke, and M. Ernzerhof, Phys. Rev. Lett. **80**, 891 (1998).

[15] W. Kohn and L. J. Sham, Phys. Rev. **140**, A1133 (1965).

[16] M. C. Payne, M. P. Teter, D. C. Allan, T. A. Arias, and J. D. Joannopoulos, Rev. Mod. Phys. **64**, 1045 (1992).

[17] A. M. Rappe, K. M. Rabe, E. Kaxiras, and J. D. Joannopoulos, Phys. Rev. B **41**, 1227 (1990).

[18] http://opium.sourceforge.net/guide.html

[19] H. J. Monkhorst and J. D. Pack, Phys. Rev. B **13**, 5188 (1976).

[20] M. Methfessel and A. T. Paxton, Phys. Rev. B **40**, 3616 (1989).

[21] C. G. Broyden, J. Inst. Math. Appl. **6**, 76 (1970); R. Fletcher, Comput. J. **13**, 317 (1970); D. Goldfarb, Math. Comput. **24**, 23 (1970); D. F. Shanno, *ibid.* **24**, 647 (1970).

[22] K. Nakamura and A. Ikawa, Phys. Rev. B **66**, 024306 (2002).

[23] E. Hernandez and Angel Rubio, Newsletter **32**, 48 (1999), http://psi-k.dl.ac.uk/newsletters/News_32/newsletter_32.pdf

[24] M. Cococcioni, F. Mauri, G. Ceder, and N. Marzari, Phys. Rev. Lett. **94**, 145501 (2005).

[25] We also evaluated the radius of Te-h, Te-w1, and Te-w2 using the definition given in Ref. 24. Using this definition, we obtain radii of Te-h, Te-w1, and Te-w2 as 3.1, 6.39, and 10.22 Å, respectively. With these values of radii, the surface energy (γ_s) for the three systems are 0.10, 0.13, and 0.15 J/m^2, respectively, and the Young's moduli (Y) are 34.46 GPa for Te-h and 40.69 GPa for Te-w1. Although the values of γ_s, and Y change depending on the definition of the radius we use, their trends as a function of the radius of nanowires are similar to our results.

[26] http://www.webelements.com

[27] N. Troullier and Jose Luis Martins, Phys. Rev. B **43**, 1993 (1991).

[28] G. Kresse, J. Furthmuller, and J. Hafner, Phys. Rev. B **50**, 13181 (1994).

[29] D. R. McCann and L. Cartz, J. Appl. Phys. **43**, 4473 (1972); W. Lingelbach, J. Stuke, G. Weiser, and J. Trensch, Phys. Rev. B **5**, 243 (1972).

[30] C. Kittel, *Introduction to Solid State Physics*, 7th ed. (Wiley, New York, 1996), pp. 57 and 59.

[31] J. D. Joannopoulos, M. Schluter, and M. L. Cohen, Phys. Rev. B **11**, 2186 (1975).

[32] C. Kittel, *Introduction to Solid State Physics*, 7th ed. (Wiley, New York, 1996), p. 201.

[33] A. Kokalj, XCRYSDEN, a new program for displaying crystalline structures and electron densities, J. Mol. Graphics Modell. **17**, 176 (1999). Code available from http://www.xcrysden.org/

[34] R. Kubo, J. Phys. Soc. Jpn. **12**, 570 (1957).

[35] D. A. Greenwood, Proc. Phys. Soc. London **71**, 585 (1958).

[36] S. Tutihasi, G. G. Roberts, R. C. Keezer, and R. E. Drews, Phys. Rev. **177**, 1143 (1969).

[37] Th. Starkloff and J. D. Joannopoulos, Phys. Rev. B **19**, 1077 (1979).